3-D Reflectarray Unit Cell with Wideband Performance and Integrated Sensing Capability

Ángel Palomares-Caballero, Carlos Molero, Pablo Padilla, María García-Vigueras, Raphaël Gillard

3-D Reflectarray Unit Cell with Wideband Performance and Integrated Sensing Capability

Ángel Palomares-Caballero*, Carlos Molero†, Pablo Padilla†, María García-Vigueras*, Raphaël Gillard*
*Institut d'Electronique et des Technologies du numéRique (IETR), UMR CNRS 6164, INSA Rennes, France
†Department of Signal Theory, Telematics and Communications, Centre for Information and Communication Technologies (CITIC-UGR), University of Granada, 18071 Granada, Spain
e-mail: Angel.Palomares-Caballero2@insa-rennes.fr

***Abstract*—A reflectarray unit cell design with sensing capability at millimeter-wave frequencies is presented in this paper. The proposed unit cell is based on slotlines spatially arranged in 3-D. There are different parts that conform the reflectarray unit cell, these are: an impedance transformer, a main slotline, an EBG filter and a sensing zone. By modifying the length of the main slotline, phase tuning of the reflected wave is achieved while preserving good level of reflection. Moreover, the phase response is linear in the frequency range that goes from 30 GHz to 50 GHz. To implement the sensing function, the EBG filter is placed after the main slotline to allow some level of leakage through the unit cell. The simulated results show that depending on the angular direction of an incident wave, there is a certain phase difference value among the sensors located in the sensing zone of the unit cell.**

***Index Terms*—3-D unit cell, millimeter-waves reflectarray, sensing capability, slotline, wideband.**

I. Introduction

A reflectarray (RA) can be seen as a type of antenna that combines certain features that are typically associated to phased arrays and reflectors [1]. On the one hand, as in phased arrays, discrete elements are arranged in the RA surface providing desired phase delay patterns. On the other hand, as in reflector antennas, the way of feeding the RA is by means of an external primary source. From the first RA antenna proposed in 1963, a wide variety of RA designs have been published using different technologies [2]–[5] and in different frequency bands , from the microwaves to the terahertz frequencies [6], [7].

Recently, the use of periodic structures with three-dimensional (3-D) geometries are proposed widely [8]. The reason behind this trend is the advantage gained in the design process as they provide an additional spatial degree of freedom. In general, this allows the possibility of achieving a design with better electromagnetic performance or additional functionalities. For example, in [9], a spatial filter made with 3-D periodic structures for two polarizations is presented. In [10], the design of a metal-only wideband polarizer is shown. The design of RA unit cells with 3-D geometry is starting to be used as presented in the work [11], where a dipole is inserted with a delay line in the direction of propagation. In [12], the design of a metal-only RA with phase-independent modification capability of linear polarizations over a large bandwidth is introduced. An example of the use of 3-D structures is also found in [13], which presents a metal-only RA with phase-independent control for circular polarizations. Another interesting design about 3-D unit cells for RAs is presented in [14] where slotlines with different lengths are employed to achieve the phase shift in the RA elements.

With the appearance of a new communication paradigm based on reconfigurable intelligent surface (RIS) [15], the fact of using reconfigurable RA with discrete phase states is receiving a lot of attention. In addition, the RIS must know the angular direction from which it receives the electromagnetic (EM) wave in order to provide an optimal performance for the reflection. One of the ways to acquire this angular information is to perform a sensing of the incident wave in the RIS or reconfigurable RA [16]. In this manner, by means of phase differences captured by sensors integrated in the unit cells, the angle of arrival can be estimated and thus, the angular position of the users. So far, there are reported only a few unit cells with this dual functionality [17], [18]: i) to provide the required phase shift for the reflected wave and ii) to be able to acquire part of power of the incident wave power for sensing purposes. However, in the previous works, broadband performance for the reflected wave is hardly achieved.

In this paper, we present the design of a RA unit cell with 3-D geometry that performs a wideband phase tuning for the reflected wave as well as the sensing of the incident wave. The paper is organized as follows. Section II describes the design of each of the parts that constitute the proposed RA unit cell. Section III presents the EM performance of the RA unit cell in both its RA and sensing functions. Finally, the conclusions are drawn in Section IV.

II. RA Unit Cell

The RA unit cell proposed is displayed in Fig. 1. The unit cell is based on slotlines as the design presented in [14]. Unlike previous work, in the present design we can identify different parts where each one has an EM purpose. In the following sections, we describe and EM characterize each of these parts, which are indicated in Fig. 1. The yellow parts in Fig. 1 are metal (copper in this case) and the brown areas represent a substrate, specifically, the RO4003C substrate (relative permittivity is 3.55 and loss tangent is 0.0027 at 10 GHz). For the EM simulations of this unit cell, CST Studio Suite software has been used. The boundary conditions applied

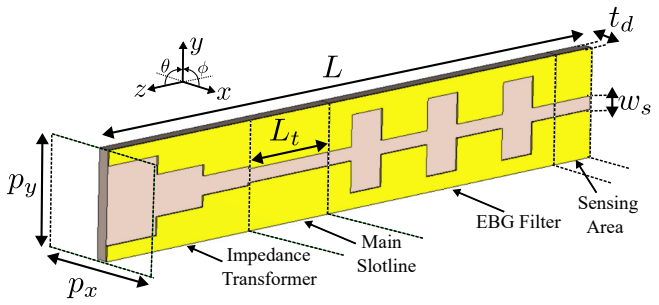

Fig. 1. 3-D view of the proposed RA unit cell. The dimensions are (in mm): $p_x = 2.75$, $p_y = 2.75$, $L = 15.9$, $w_s = 0.35$ and, $t_d = 0.305$.

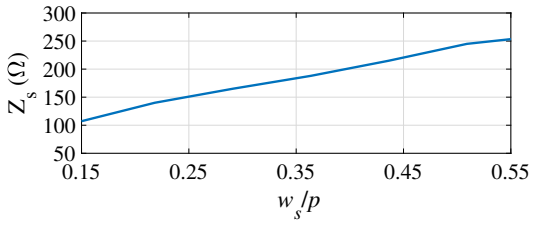

Fig. 2. Characteristic impedance of the slotline as a function of its width. The parameter p stands for $p_x = p_y$.

in the simulations are *unit cell* in the x- and y- directions, and *open add space* in the z-direction. The excitation considered is a plane wave propagating in the $-z$-direction and the electric field (E-field) is aligned to the y-direction.

A. Impedance Transformer

When a plane wave impinges on the RA unit cell of Fig. 1, it firstly interacts with an impedance transformer. Since the purpose of this part of the unit cell is to maximize power transfer to the main slotline, an impedance matching from free space to the main slotline is needed. Classical transmission line theory can be used to design an impedance transformer [19]. For this, it is needed to know the dependence of the characteristic impedance of the slotline Z_s with respect to the slot width w_s. Such a relation is shown in Fig. 2, and the geometrical parameters are normalized to the unit cell period [10]. The width of the main slotline is 0.35 mm and this corresponds to a Z_s value of 101Ω ($w_s/p = 0.127$). Using such information, a broadband impedance transformer can be designed considering three sections of identical length L_{tr} with the appropriate Z_s values. A three-section binomial transformer is selected due to its simplicity and its balance between compactness and required matching performance. To check the performance of the designed impedance transformer, Fig. 3 shows the S-parameters of a back-to-back design based on a slotline with these transformers placed at its ends. A S_{11} around -20 dB with a S_{21} higher than -0.3 dB is achieved from 30 GHz to 50 GHz.

B. EBG Filter

In Fig. 1, after the main slotline, which controls the phase shift introduced in reflection by the unit cell, it is located the

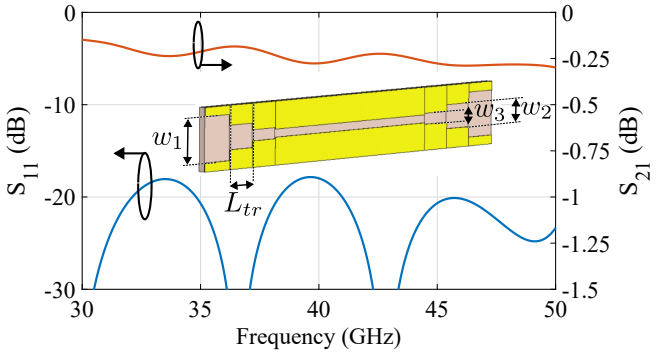

Fig. 3. S-parameters of a slotline whose ends have a broadband impedance transformer. The dimensions are (in mm): $w_1 = 1.975$, $w_2 = 1.05$, $w_3 = 0.48$, and $L_{tr} = 1.5$.

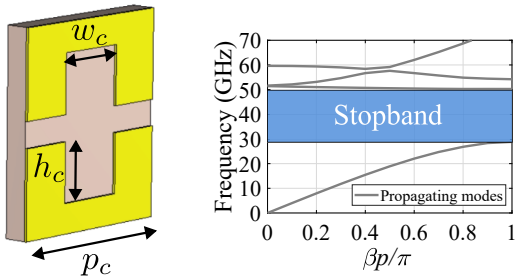

(a) (b)

Fig. 4. EBG unit cell based on slotline. (a) 3-D view of the design and, (b) Dispersion diagram in the z-direction. The dimensions are (in mm): $w_c = 1$, $h_c = 0.8$ and, $p_c = 2.5$.

electromagnetic bandgap (EBG) filter. The purpose of this part is to reflect most of the incident power arriving at the end of the main slotline while still allowing some control over the power leakage to the sensing area. For the design of the EBG filter, it is necessary to design a unit cell that provides a stopband in the operating frequency band, which is from 30 GHz to 50 GHz. Figs. 4(a) and (b) show the design of the EBG unit cell and its dispersion diagram, respectively. Through the inclusion of symmetric corrugations in the slotline, a stopband can be produced in the propagation direction [20]. To check the EM performance of the EBG filter, the S-parameters of a back-to-back design are assessed as in Fig. 3 but in this case, EBG unit cells are included in the central slotline. In Fig. 5, the S-parameters of this back-to-back design are shown depending on the number of EBG unit cells used. Also included in this figure, there is a representation of the E-field distribution when three EBG unit cells are used. It can be seen that as the number of EBG unit cells increases, the S_{21} decreases and in a complementary way, the S_{11} increases. In this manner, we can choose the level of power we want to acquire with the sensor located after the EBG filter.

III. EM PERFORMANCE OF THE PROPOSED UNIT CELL

Once the parts that compose the proposed RA unit cell have been described, this section will present the EM performance

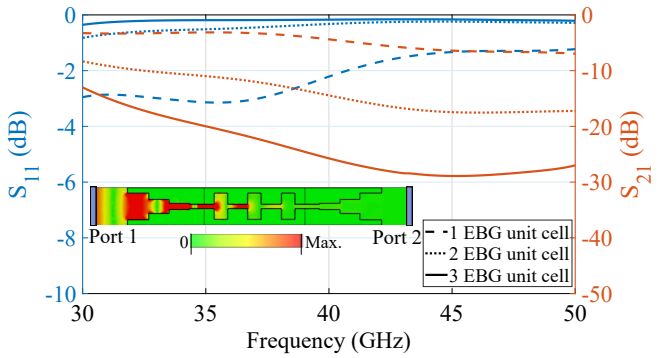

Fig. 5. S-parameters of a slotline with broadband impedance transformers and different number of EBG unit cells placed at the middle of the slotline. The inset represents the magnitude of the E-field when 3 EBG unit cells are used.

of the complete unit cell, i.e., the RA unit cell illustrated in Fig. 1.

A. RA function

The proposed RA unit cell allows to modify the phase of the reflected wave by varying the length L_t of the main slotline [see Fig. 1]. Figs. 6(a) and (b) present the reflection response in magnitude and phase, respectively, for different values of L_t in a normal incidence situation ($\phi = 0^o$, $\theta = 0^o$). Regarding the response in magnitude, a reflection level greater than -0.5 dB is obtained for the whole range of L_t values. It is important to say that the S_{11} is not 0 dB due to the existence of losses in the dielectric and metal of the structure and, due to the desired leakage of power through the EBG filter. Regarding the phase behavior, we can see that a linear response is achieved along the frequency range for the whole range of L_t. Moreover, the phase curves for each value of L_t are quasi-parallel to each other which denotes, taking into account the linear phase response in frequency, a wideband behavior for the RA unit cell. At the central frequency of the considered bandwidth, a 360º phase shift range is achieved, which is important for a proper RA design.

Having analyzed the proposed RA unit cell for normal incidence, we extend this analysis to oblique incidence. Figs. 7 and 8 show the magnitude and phase response for different values of L_t at TE and TM oblique incidence, respectively. Taking into account the axis shown in Fig. 1, the TE incidence is considered when the direction of the incident wave is $\phi = 0^o$ and θ varies; and TM incidence is produced when $\phi = 90^o$ and the value of θ is modified. In the Figs. 7 and 8, the angle of incidence θ is varied from 15º to 45º. Observing the results, it can be said that the RA unit cell preserves the desired performance for TE incidence since the response in magnitude and phase along the frequency is very similar to that described for normal incidence. For TM incidence (Fig. 8), resonances begin to appear in the magnitude response which are dependent with the value of θ. In addition, the linear behavior of the phase response along the frequency deteriorates as can be seen in Fig. 8(d). This is due to the

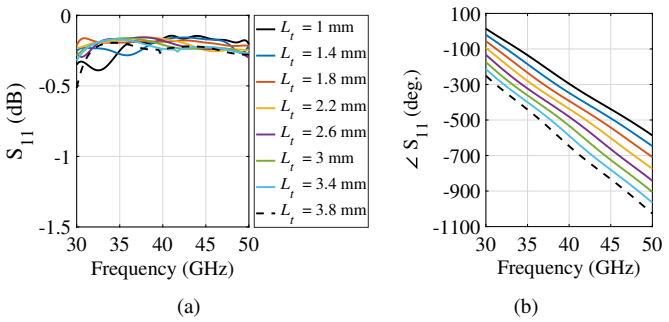

Fig. 6. Reflection performance, at normal incidence ($\phi = 0^o$, $\theta = 0^o$), of the RA unit cell when the L_t parameter is swept: (a) in magnitude and, (b) in phase.

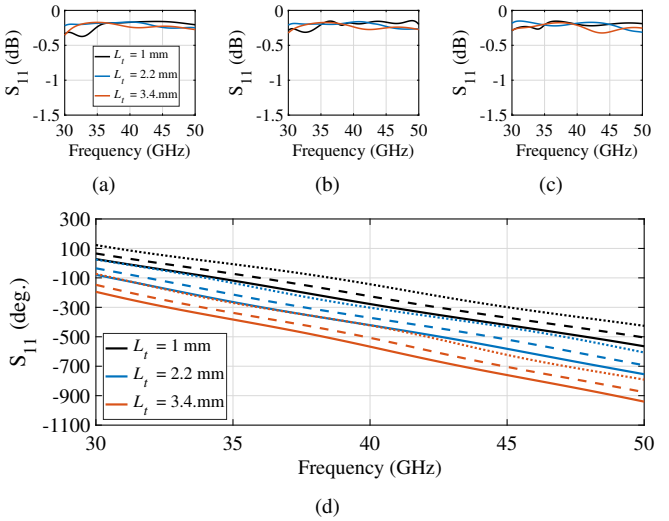

Fig. 7. Reflection performance of the RA unit cell for some L_t values under different oblique angles (θ) when $\phi = 0^o$ (TE incidence). In magnitude when (a) $\theta = 15^o$, (b) $\theta = 30^o$ and, (c) $\theta = 45^o$. (d) In phase where the solid, dashed and dotted lines correspond to $\theta = 15^o$, $\theta = 30^o$ and, $\theta = 45^o$, respectively.

excitation of unwanted modes between the neighboring unit cells in the x-direction. In this direction, there are air zones separating the unit cells as illustrated in Fig. 9(a). In order to mitigate these resonances, one strategy is to reduce the value of the parameter p_x.

B. Sensing function

In order to electromagnetically evaluate the sensing function provided by the proposed unit cell, a 1x4 array of RA unit cells is considered where, in the so-called sensing area [see Fig. 1], a sensor is placed. This can be thought of as an element that can capture the phase and magnitude of the incident wave, such as a port of a network analyzer. The described design is illustrated in Fig. 9(a). For this design, a plane wave excitation is considered where the incidence angle θ is modified in a TE incidence situation. First, it should be found that the implementation of sensors at the end of the RA unit cell has no influence for the RA function. This fact is shown in Figs. 9(b) and 9(c) which present the magnitude

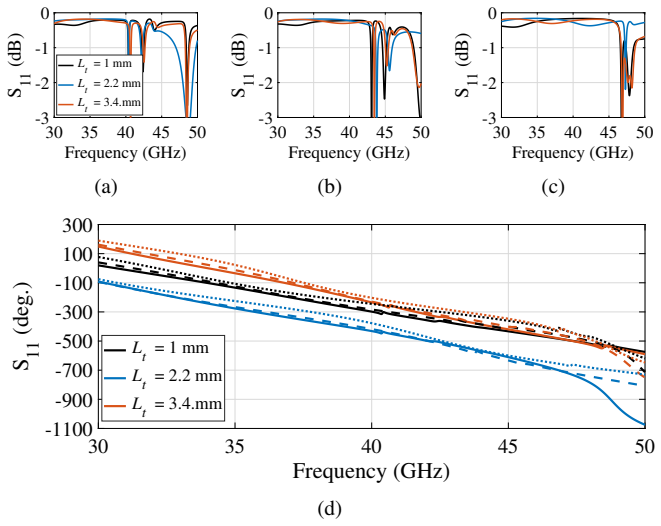

Fig. 8. Reflection performance of the RA unit cell for some L_t values under different oblique angles (θ) when $\phi = 90^o$ (TM incidence). In magnitude when (a) $\theta = 15^o$, (b) $\theta = 30^o$ and, (c) $\theta = 45^o$. (d) In phase where the solid, dashed and dotted lines correspond to $\theta = 15^o$, $\theta = 30^o$ and, $\theta = 45^o$, respectively.

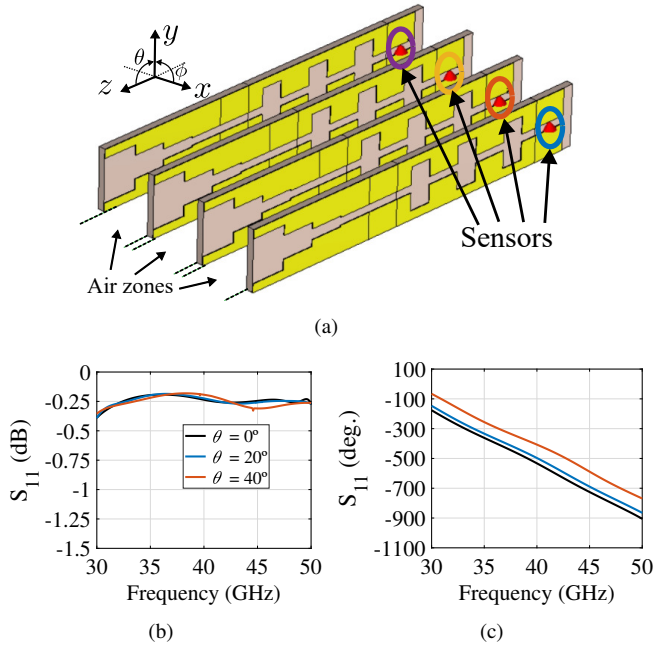

Fig. 9. (a) 3-D view of an array of 1x4 RA unit cells with sensors. Unit cell boundaries are set for $x-$ and $y-$ directions. (b) Reflection performance of the array of RA unit cells under different oblique angles (θ) when $\phi = 0^o$: (b) in magnitude and, (c) in phase.

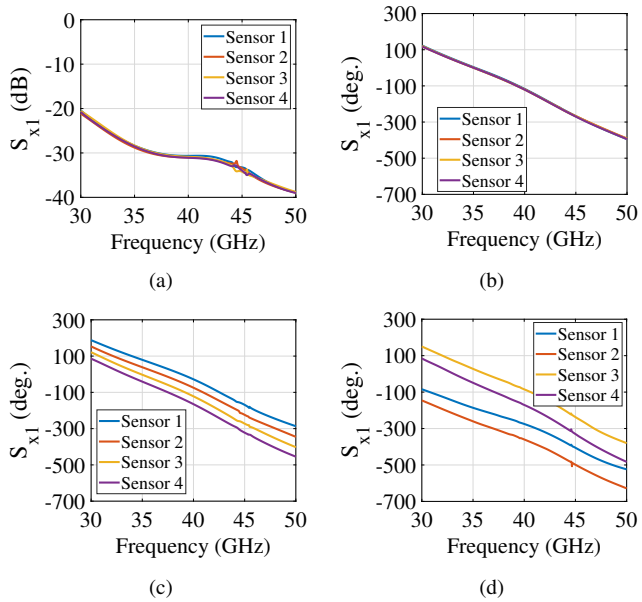

Fig. 10. S-parameters of the sensors illustrated in Fig. 9(a). (a) In magnitude when the incident wave has an angular direction of $\phi = 0^o$ and $\theta = 20^o$. In phase when the incident wave has an angular direction of $\phi = 0^o$ and (b) $\theta = 0^o$, (c) $\theta = 20^o$ and, (d) $\theta = 40^o$.

and phase responses, respectively, of the reflected wave for different values of θ. These results are very similar to those presented in Fig. 7. Once this fact is verified, we perform an S-parameters analysis of the sensors for different values of θ. The results in both magnitude and phase for three different angle values are illustrated in Fig. 10. In the simulations carried out to obtain these results, an excitation power of 0.5 W (-3.01 dBW) has been considered. Therefore, the S-parameters in magnitude show how much of the incident power is captured by the sensors. The magnitude response is presented in Fig. 10(a), where we can see that there is practically no difference in the power level among the sensors. In addition, the power level captured by the sensors is approximately 30 dB lower than the power level of the reflected wave shown in Fig. 9(b). It is important to note that this power level captured by the sensors can be higher if fewer unit cells are used in the EBG filter.

Figs. 10(b), 10(c) and 10(d) show the phase responses captured by the sensors in each of the oblique incident situation. It is observed that depending on the value of θ of the incident wave, there is a phase difference between sensors that remains more or less constant with the frequency. It is worth pointing that this difference is not affected by the length of the main slotlines which compose the array of unit cells. Moreover, as the value of θ increases, this phase difference becomes larger so this fact can be used to estimate the angular direction by computing the phase differences between sensors in a certain frequency band.

IV. Conclusion

In this paper, it is presented a RA unit cell design with wideband performance in millimeter-waves and with sensing capability of the impinging wave. The proposed RA unit cell is based on slotlines whose width is modified to implement different parts in the design with a given EM purpose. The RA unit cell design can be divided into four parts: an impedance transformer, a main slotline, a filter based on EBG structures and a sensing area. By modifying the length of the main slotline, the phase of the reflected wave can be modified over a

large bandwidth which ranges from 30 GHz to 50 GHz. In fact, the behavior of the reflected phase is linear over the frequency for the possible length values in the main slotline. Moreover, a modification of the reflection phase value of 360º is achieved. The unit cell behavior in frequency allows the design of a reflectarray with large bandwidth. For the implementation of the sensing function, an EBG filter has been designed which allows a certain level of leakage into a slotline section, named sensing area, located after this filter. Depending on the number of EBG unit cells used to implement the filter, a certain level of transmission to the sensing area is achieved. Simulations of an array of 1x4 RA unit cells, where each of them has a sensor in the sensing area, have been carried out. It has been observed that depending on the angle of the incident wave on the array, certain phase differences are captured in the sensors. Through the computation of these differences in a certain frequency range, the angle of the incident wave can be easily estimated.

ACKNOWLEDGMENT

This work has been supported by the Brittany Region under Contract SAD 22006912 (SuMeRIO). It has also been supported by the grant PID2020-112545RB-C54, grants PDC2022-133900-I00, TED2021-129938B-I00, TED2021-131699B-I00 and IJC2020-043599-I funded by MCIN/AEI/10.13039/501100011033 and by the European Union NextGenerationEUPRTR.

REFERENCES

[1] D. Berry, R. Malech and W. Kennedy, "The reflectarray antenna," *IEEE Trans. Antennas Propag.*, vol. 11, no. 6, pp. 645-651, November 1963.

[2] M. H. Jamaluddin *et al.*, "Design, fabrication and characterization of a dielectric resonator antenna reflectarray in Ka-band," *Prog. Electromagn. Res. B*, vol. 25, pp. 261–275, 2010.

[3] E. Carrasco, M. Barba, J. A. Encinar, M. Arrebola, F. Rossi and A. Freni, "Design, manufacture and test of a low-cost shaped-beam reflectarray using a single layer of varying-sized printed dipoles," *IEEE Trans. Antennas Propag.*, vol. 61, no. 6, pp. 3077-3085, June 2013.

[4] R. Deng, F. Yang, S. Xu and M. Li, "A low-cost metal-only reflectarray using modified slot-type phoenix element with 360º phase coverage," *IEEE Trans. Antennas Propag.*, vol. 64, no. 4, pp. 1556-1560, April 2016.

[5] C. Kocia and S. V. Hum, "Design of an optically transparent reflectarray for solar applications using indium tin oxide," *IEEE Trans. Antennas Propag.*, vol. 64, no. 7, pp. 2884-2893, July 2016.

[6] P. I. Theoharis, R. Raad, F. Tubbal, M. U. A. Khan and A. Jamalipour, "Wideband reflectarrays for 5G/6G: a survey," *IEEE Open J. Antennas Propag.*, vol. 3, pp. 871-901, 2022.

[7] P. Hosseini and O. Homayoon, "Analysis and design of terahertz reflectarrays based on graphene cell clusters," *Sci. Rep.*, vol. 12, no. 1, p. 22117, Dec. 2022.

[8] A. Alex-Amor, Á. Palomares-Caballero and C. Molero, "3-D metamaterials: trends on applied designs, computational methods and fabrication techniques," *Electronics*, vol. 11, no. 3, p. 410, Jan. 2022.

[9] J. Zhu, W. Tang, C. Wang, C. Huang and Y. Shi, "Dual-polarized bandpass frequency-selective surface with quasi-elliptic response based on square coaxial waveguide," *IEEE Trans. Antennas Propag.*, vol. 66, no. 3, pp. 1331-1339, March 2018.

[10] C. Molero, H. Legay, T. Pierré and M. García-Vigueras, "Broadband 3D-printed polarizer based on metallic transverse electromagnetic unit-cells," *IEEE Trans. Antennas Propag.*, vol. 70, no. 6, pp. 4632-4644, June 2022.

[11] W. Li, S. Gao, L. Zhang, Q. Luo and Y. Cai, "An ultra-wide-band tightly coupled dipole reflectarray antenna," *IEEE Trans. Antennas Propag.*, vol. 66, no. 2, pp. 533-540, Feb. 2018.

[12] Á. Palomares-Caballero, C. Molero, P. Padilla, M. García-Vigueras and R. Gillard, "Wideband 3-D-printed metal-only reflectarray for controlling orthogonal linear polarizations," *IEEE Trans. Antennas Propag.*, vol. 71, no. 3, pp. 2247-2258, March 2023.

[13] J. Zhu, S. Liao, S. Li and Q. Xue, "Additively manufactured metal-only millimeter-wave dual circularly polarized reflectarray antenna with independent control of polarizations," *IEEE Trans. Antennas Propag.*, vol. 70, no. 10, pp. 9918-9923, Oct. 2022.

[14] T.-X. Feng, L. Zhu, X. Zhao and B. Li, "3-D pattern modulation surfaces using short-circuited slotline structure: proposal, design, and implementation," *IEEE Trans. Antennas Propag.*, vol. 70, no. 10, pp. 8739–8747, Oct. 2022.

[15] Y. Liu *et al.*, "Reconfigurable intelligent surfaces: principles and opportunities," *IEEE Commun. Surv. Tutor.*, vol. 23, no. 3, pp. 1546-1577, thirdquarter 2021.

[16] I. Alamzadeh and M. F. Imani, "Sensing and reconfigurable reflection of electromagnetic waves from a metasurface with sparse sensing elements," *IEEE Access*, vol. 10, pp. 105954-105965, 2022.

[17] I. Alamzadeh, G. C. Alexandropoulos, N. Shlezinger, and M. F. Imani, "A reconfigurable intelligent surface with integrated sensing capability," *Sci. Rep.*, vol. 11, no. 1, p. 20737, Oct. 2021.

[18] M. Hwang *et al.*, "Demonstration of millimeter-Wave reconfigurable intelligent surface (RIS) with built-in sensors for automatic tracking of direction-of-arrival (DOA)," *IEEE Sens. Lett.*, vol. 7, no. 8, pp. 1-4, Aug. 2023, Art no. 7003704.

[19] D. Pozar, *Microwave Engineering*, 4th ed. Hoboken, NJ, USA: Wiley, 2004.

[20] R. Quesada, D. Martín-Cano, F. J. García-Vidal, and J. Bravo-Abad, "Deep-subwavelength negative-index waveguiding enabled by coupled conformal surface plasmons," *Opt. Lett.*, vol. 39, no. 10, p. 2990, May 2014.